Decoupled and Modular Torque Control of Multi-Three-Phase Induction Motor Drives

Decoupled and Modular Torque Control of Multi-Three-Phase Induction Motor Drives

Sandro Rubino, Radu Bojoi, Davide Cittanti
Dipartimento Energia
"G. Ferraris"
Politecnico di Torino
Torino, Italy
sandro.rubino@polito.it

Luca Zarri
Dept. of Electrical, Electronic and
Information Engineering "G. Marconi"
University of Bologna
Bologna, Italy
luca.zarri2@unibo.it

***Abstract*—In recent years, the development of multi-three-phase drives for both energy production and transportation electrification has gained growing attention. An essential feature of the multi-three-phase drives is their modularity since they can be configured as three-phase units operating in parallel and with a modular control scheme. The so-called multi-stator modeling approach represents a suitable solution for the implementation of modular control strategies able to deal with several three-phase units. Nevertheless, the use of the multi-stator approach leads to relevant coupling terms in the resulting set of equations. To solve this issue, a new decoupling transformation for the decoupled torque control of multi-three-phase induction motor drives is proposed. The experimental validation has been carried out with a modular power converter feeding a twelve-phase induction machine prototype (10 kW, 6000 rpm) using a quadruple three-phase stator winding configuration.**

Keywords— multiphase electrical machines, multiphase motor drives, direct flux vector control, induction motor drives.

I. INTRODUCTION

Thanks to the advancements in power electronics, the multi-three-phase drives are playing a pivotal role in the development of multiphase solutions for both energy production and transportation electrification [1]–[5]. The stator of a multi-three-phase machine consists of independent three-phase windings with isolated neutral points. Each winding set is fed by a standalone three-phase ac/dc converter, as shown in Fig. 1. Several advantages of this multiphase drive topology can be emphasized. The first one is the possibility to use the consolidated three-phase technologies, thus reducing the converter cost and design time [2]. Another advantage consists of the opportunity to obtain drive modularity for fault-tolerant control. Indeed, in case of an open-phase fault event, the faulty three-phase unit is disconnected from the dc power supply, thus allowing a straightforward post-fault drive reconfiguration.

The multi-three-phase machines can be modeled with several approaches. The most employed one is the Vector Space Decomposition (VSD) approach. The VSD models the electromechanical energy conversion as in a conventional three-phase machine [6], [7], thus leading to an average machine model. Despite the simplicity of the results, the VSD modeling is not able to emphasize the flux and torque contributions of the single three-phase sets. Therefore, this approach is not recommended when modular control schemes need to be implemented, as happens for multi-three-phase motor drives. The modularity of the torque control for a multi-three-phase machine is obtained if the torque contribution of each three-phase machine set is independently controlled and decoupled from the torque contributions of the other sets. The literature reports some VSD-based Direct Torque Control (DTC) solutions [8]–[10].

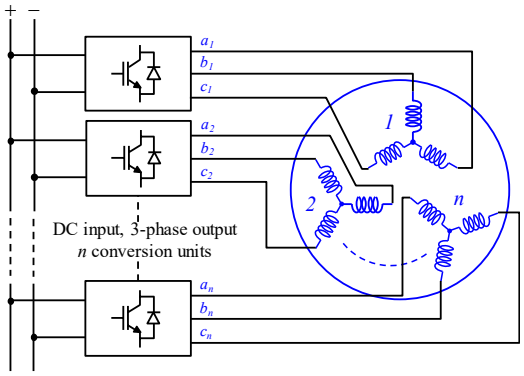

Fig. 1. Multi-three-phase drive topology.

However, due to the lack of modularity of the VSD model, no solutions able to compute the stator flux amplitude and torque references after an open-three-phase fault have been developed.

A possible alternative to VSD modeling is the Multi-Stator (MS) approach [1], [11], which represents the machine as multiple three-phase stator sets interacting with each other and with the three-phase rotor. This approach highlights the contributions to the machine flux and torque provided by each three-phase winding set, so it is suitable for the implementation of modular control schemes with direct control of each three-phase unit [1], [12].

In recent years, several MS-based torque control schemes have been proposed [12]–[15]. Except for [15], these solutions use the Direct Flux Vector Control (DFVC) approach for direct flux amplitude regulation and with torque control through the regulation of the torque-producing stator current components [16].

Besides the excellent torque control performance, including deep flux-weakening operation with Maximum Torque per Volt (MTPV), the main advantage of the MS-based torque control schemes [12]–[14] is their straightforward reconfiguration after an open-three-phase fault event. Indeed, the use of the MS approach allows a straightforward computation of the stator flux amplitude and torque references of the healthy winding sets. However, these solutions require demanding control algorithms to compensate for the couplings between the three-phase sets introduced by MS modeling [12]. Without a proper decoupling [17], the coupling terms can lead to instability, as reported in [18].

Recently, some solutions have been proposed in the literature to remove the coupling terms resulting from the MS modeling, using dedicated reference frame transformations [19]–[21]. The most interesting one is illustrated in [19], where a decoupling transformation was proposed only for dual three-phase machines, thus having limited generality. The control scheme proposed in [19] is based on the conventional Field-Oriented Control (FOC) with inner current regulation loops.

Based on the authors' best knowledge, no MS decoupling transformation has been proposed for multi-three-phase machines having a generic number of three-phase winding sets. The advantages of such a reference frame transformation are evident since it may combine the main features of VSD and MS approaches in terms of simplicity of the equations and modularity, respectively.

Therefore, the goal of this work is to extend the solution from [19], by proposing a new decoupling transformation able to deal with multi-three-phase machines having an arbitrary number of three-phase winding sets.

The new decoupling transformation has been employed for a decoupled and modular torque control of multi-three-phase Induction Motor (IM) drives, using a DFVC approach. In detail, the proposed solution combines the advantages of the VSD-based schemes (the decoupled control) with the ones of the MS-based schemes (the modularity and easy reconfiguration after an open-three-phase fault). The application of the new decoupling transformation leads to the following benefits:

- Full decoupling between the three-phase units (like a VSD-based scheme).
- Straightforward reconfiguration after an open-three-phase fault event (like an MS-based scheme).

The performance of the proposed control solution has been validated on a twelve-phase IM prototype, rated 10 kW at 6000 rpm, which uses a quadruple three-phase stator winding configuration. This paper extends the results that have been presented in [22] with experimental validation of the drive operation in deep flux-weakening, thus including the MTPV operation with load-angle limitation.

The paper is organized as follows. The machine modeling, together with the proposed decoupling method, is described in Section II. The control scheme is shown in Section III, while the experimental validation is illustrated in Section IV. The paper conclusion is provided in Section V.

II. Machine Modeling and Decoupling Method

The multi-three-phase IM can be modeled using both VSD, and MS approaches [17]. However, due to specific constraints on the computation of the reference transformation [23], the application of the VSD modeling is usually limited to the symmetrical and asymmetrical winding configurations. Conversely, the MS approach can be applied to any multi-three-phase machine because a three-phase Clarke transformation is used to deal with each winding set [1], [11].

In the following, the IM is assumed with sinusoidal winding distribution; the stator and rotor windings interact with each other only through the fundamental spatial component of the airgap field.

A. Vector space decomposition (VSD) approach

The VSD approach decomposes the machine space (phase-coordinates) in multiple orthogonal harmonic subspaces, using a full-order reference transformation. According to [6], the main subspace (α,β) has the meaning of the time-fundamental model of the machine that performs the electromechanical energy conversion.

Concerning the other subspaces, they have the meaning of harmonic and homopolar patterns of the machine. According to [17], [23], if a multi-three-phase machine having n three-phase winding sets is considered, the application of the VSD transformation leads to the definition of *one* main subspace, (n-1) harmonic subspaces and n zero-sequence components.

The application of the VSD transformation allows obtaining the electromagnetic machine model in stationary coordinates. Therefore, by applying the rotation transformation [24], the equations of the main subspace can be computed in a generic rotating (x,y) frame, which corresponds to the usual (d,q) frame in FOC schemes [7].

However, the rotation operation can also be extended to each harmonic (μ+,μ-) subspace, which is useful if power/torque sharing strategies among the three-phase windings sets are implemented [12], [25]–[27]. At steady-state conditions, any time-fundamental variable (current, flux, voltage) is mapped in the harmonic subspaces as a dc quantity, allowing its control through standard Proportional-Integral (PI) controllers. Concerning the zero-sequence components, these can be neglected since each three-phase winding set has an own neutral point isolated from the others.

According to [17], the electromagnetic VSD model of the main subspace in rotating (x,y) coordinates is:

$$\begin{cases} \overline{v}_{s,xy} = R_s \cdot \overline{i}_{s,xy} + \dfrac{d}{dt}\overline{\lambda}_{s,xy} + j \cdot \omega_{xy} \cdot \overline{\lambda}_{s,xy} \\ \overline{\lambda}_{s,xy} = k_r \cdot \overline{\lambda}_{r,xy} + \left(L_{ls} + k_r \cdot n \cdot L_{lr}\right) \cdot \overline{i}_{s,xy} \\ \overline{0} = \dfrac{\overline{\lambda}_{r,xy}}{\tau_r} + \dfrac{d}{dt}\overline{\lambda}_{r,xy} + j \cdot \omega_{slip} \cdot \overline{\lambda}_{r,xy} - k_r \cdot n \cdot R_r \cdot \overline{i}_{s,xy} \end{cases} \quad (1)$$

where $\overline{z}_{s,xy} = \left[z_{s,x} \;\; z_{s,y} \right]^t$ is a generic stator vector referred to the generic rotating (x,y) frame; $\overline{z}_{r,xy} = \left[z_{r,x} \;\; z_{r,y} \right]^t$ is a generic rotor vector referred to the generic rotating (x,y) frame; R_s, L_{ls}, R_r and L_{lr} represent the stator resistance, stator leakage inductance, rotor resistance, and rotor leakage inductance respectively; k_r is the rotor coupling factor; τ_r represents the rotor time constant; v, i and λ have the meaning of voltage, current, and flux linkage respectively; ω_{xy} is the synchronous speed of the (x,y) frame, ω_{slip} represents the slip speed of the (x,y) frame; j is the complex vector operator.

The electromagnetic model of each harmonic subspace h (h=1÷(n-1)) [17], referred to the rotating (x,y) frame, is computed as:

$$\begin{cases} \overline{v}_{sh,xy} = R_s \cdot \overline{i}_{sh,xy} + \dfrac{d}{dt}\overline{\lambda}_{sh,xy} + j \cdot \omega_{xy} \cdot \overline{\lambda}_{sh,xy} \\ \overline{\lambda}_{sh,xy} = L_{ls} \cdot \overline{i}_{sh,xy} \\ \overline{0} = \left(R_r / L_{lr}\right) \cdot \overline{\lambda}_{rh,xy} + \dfrac{d}{dt}\overline{\lambda}_{rh,xy} + j \cdot \omega_{xy} \cdot \overline{\lambda}_{rh,xy} \end{cases} \quad (2)$$

where $\overline{z}_{sh,xy} = \left[z_{sh,x} \;\; z_{sh,y} \right]^t$ is a generic harmonic stator vector referred to the generic rotating (x,y) frame; $\overline{z}_{rh,xy} = \left[z_{rh,x} \;\; z_{rh,y} \right]^t$ is a generic harmonic rotor vector referred to the generic rotating (x,y) frame. Finally, the IM electromagnetic torque T is computed as follows:

$$T = \frac{3 \cdot n}{2} \cdot p \cdot \left(\overline{\lambda}_{s,xy} \times \overline{i}_{s,xy} \right) \quad (3)$$

where p represents the pole pair number of the machine. According to (3), the electromagnetic torque is given by the cross product between the stator flux linkage vector and stator current vector, both belonging to the main subspace. Therefore, the equivalent circuit of the IM corresponding to the VSD approach is shown in Fig. 2, where L_m represents the magnetizing inductance, and ω_r is the rotor electrical speed.

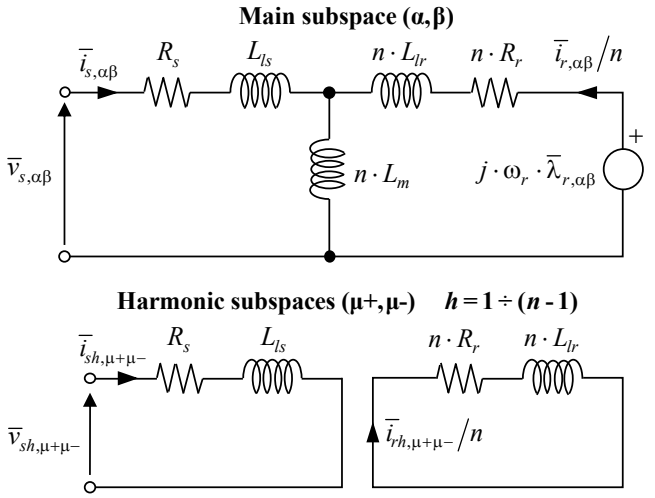

Fig. 2. Equivalent VSD circuit of a multi-three-phase squirrel cage IM in stationary coordinates (zero-sequence components not considered).

The VSD approach leads to a simple electromagnetic model of the machine, but it does not emphasize the flux and torque contributions of each single three-phase winding set.

B. Multi-stator (MS) approach

The MS approach decomposes the machine space (phase-coordinates) in multiple parallel time-fundamental (αβ0) models. A dedicated Clarke transformation is applied to each set k [24]. Therefore, for the k^{th} set, a specific (α,β) subspace plus a zero-sequence component is defined. The (α,β) subspace of the k^{th} set contributes to the flux and torque production [1], [11], thus obtaining a modular machine model. Therefore, the MS approach leads to the computation of n stator complex electromagnetic equation systems. As with VSD modeling, they can be transformed into a generic rotating (x,y) frame. From [12], [13], [17], the electromagnetic model of a generic set k (k=1÷n) is:

$$\begin{cases} \bar{v}_{sk,xy} = R_s \cdot \bar{i}_{sk,xy} + \dfrac{d}{dt}\bar{\lambda}_{sk,xy} + j \cdot \omega_{xy} \cdot \bar{\lambda}_{sk,xy} \\ \bar{\lambda}_{sk,xy} = k_r \cdot \bar{\lambda}_{r,xy} + L_{ls} \cdot \bar{i}_{sk,xy} + k_r \cdot L_{lr} \cdot \sum_{l=1}^{n} \bar{i}_{sl,xy} \\ \bar{0} = \dfrac{\bar{\lambda}_{r,xy}}{\tau_r} + \dfrac{d}{dt}\bar{\lambda}_{r,xy} + j \cdot \omega_{slip} \cdot \bar{\lambda}_{r,xy} - k_r \cdot R_r \cdot \sum_{l=1}^{n} \bar{i}_{sl,xy} \end{cases} \quad (4)$$

where $\bar{z}_{sk,xy} = \left[z_{sk,x} \;\; z_{sk,y} \right]^t$ is a generic stator vector defined for the three-phase set k and referred to the generic rotating (x,y) frame, while $\bar{z}_{sl,xy} = \left[z_{sl,x} \;\; z_{sl,y} \right]^t$ is a generic stator vector defined for the three-phase set l and referred to the generic rotating (x,y) frame. In this case, the IM electromagnetic torque is computed as:

$$T = \sum_{k=1}^{n} T_k = \frac{3}{2} \cdot p \cdot \sum_{k=1}^{n} \left(\bar{\lambda}_{sk,xy} \times \bar{i}_{sk,xy} \right) \quad (5)$$

where T_k is the k-set electromagnetic torque contribution. According to (5), the electromagnetic torque is the sum of the contributions of the n stator sets that interact with the three-phase rotor. Each k-set contribution is given by the cross-product between the k-set stator flux linkage vector and the k-set stator current vector, highlighting the full modularity of the MS approach.

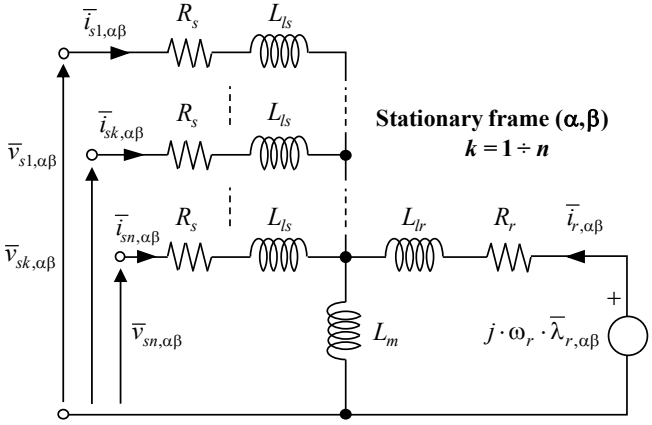

Fig. 3. Equivalent MS circuit of a multi-three-phase squirrel cage IM in stationary coordinates (zero-sequence components not considered).

Therefore, the equivalent circuit of the IM corresponding to the MS modeling is shown in Fig. 3. Finally, it can be noted that the MS approach results in a 'modular' machine model, however, characterized by strong magnetic couplings among the three-phase winding sets.

C. Decoupling method applied to the MS approach

Starting from the MS machine model, the proposed decoupling method introduces a further reference frame transformation able to remove the magnetic couplings between the winding sets. In this way, the resulting electromagnetic model of the machine becomes similar to that obtained using the VSD approach (1)-(3). However, because the new model is built starting from the MS modeling, the modularity is preserved.

According to the literature, the decoupling methods can be defined using several approaches [19], [21]. In this work, the computation of the common and differential modes of the machine is proposed. The main goal is to concentrate the energy conversion in a common-mode subspace, while the unbalances between the three-phase sets in terms of flux and torque production are mapped in specific differential-mode subspaces. In this way, the decoupling action can be performed in any generic rotating frame, thus allowing its implementation on different MS-based control schemes.

For a multi-three-phase machine having n winding sets, *one* common subspace and (n-1) differential subspaces can be identified. These subspaces should be defined so that they are independent and decoupled from each other. Therefore, for a generic stator variable of the machine z_s (flux linkage, current, voltage), *one* common-mode vector $\bar{z}_{scm}$, and (n-1) differential-mode vectors $\bar{z}_{sdm-u}$ (u=1÷(n-1)) are defined.

For example, let us consider a generic stator vector $\bar{z}_{sk,xy}$ defined for the set k (k=1÷n) and referred to the generic rotating (x,y) frame. It is possible to demonstrate how, according to the following equation, this can be expressed as a linear combination of the common and differential vectors as:

$$\bar{z}_{sk,xy} = \bar{z}_{scm,xy} + w_k \cdot \bar{z}_{sdm-k,xy} + \sum_{\substack{u=1 \\ u \neq k}}^{k} \left(q_u \cdot \bar{z}_{sdm-u,xy} \right) \quad (6)$$

where the coefficients w_k and q_u are defined as:

$$w_k = \sqrt{\frac{n \cdot (n-k)}{(n-k+1)}} \quad , \quad q_u = -\sqrt{\frac{n}{(n-u) \cdot (n-u+1)}} \quad (7)$$

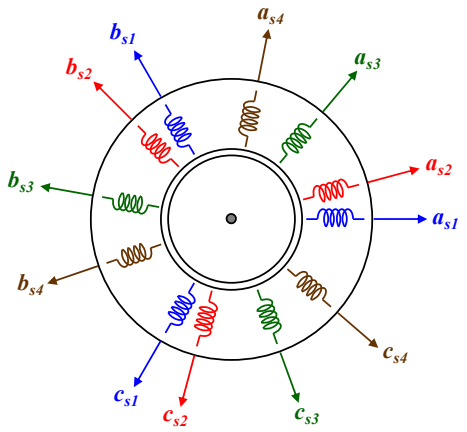

Fig. 4. Generic quadruple three-phase ac machine configuration.

It can be noted that the common and differential vectors must be referred to the same reference frame of the considered stator vector $\bar{z}_{sk}$. By merging (6) for all sets k=1÷n, the following linear transformation is defined:

$$\begin{Bmatrix} \bar{z}_{s1,xy} \\ \bar{z}_{s2,xy} \\ \dots \\ \bar{z}_{sn,xy} \end{Bmatrix} = [T_d]^{-1} \cdot \begin{Bmatrix} \bar{z}_{scm,xy} \\ \bar{z}_{sdm-1,xy} \\ \dots \\ \bar{z}_{sdm-(n-1),xy} \end{Bmatrix} \tag{8}$$

where the decoupling transformation matrix $[T_d]$ is

$$[T_d] = \frac{1}{n} \cdot \begin{bmatrix} 1 & 1 & 1 & 1 & \dots & 1 & 1 & 1 & 1 \\ w_1 & q_1 & q_1 & q_1 & \dots & q_1 & q_1 & q_1 & q_1 \\ 0 & w_2 & q_2 & q_2 & \dots & q_2 & q_2 & q_2 & q_2 \\ 0 & 0 & w_3 & q_3 & \dots & q_3 & q_3 & q_3 & q_3 \\ \dots & \dots & \dots & \dots & \dots & \dots & \dots & \dots & \dots \\ 0 & 0 & 0 & 0 & \dots & 0 & w_{n-2} & q_{n-2} & q_{n-2} \\ 0 & 0 & 0 & 0 & \dots & 0 & 0 & w_{n-1} & q_{n-1} \end{bmatrix} \tag{9}$$

The proposed decoupling transformation consists of a sparse matrix easy to implement on commercial digital controllers. Moreover, it is characterized by the amplitude invariant feature with a power coefficient equal to n. For example, by computing (9) for a quadruple three-phase ac machine, like the one used for the experimental validation, the following transformation matrix is obtained:

$$[T_d]_{4\times 3} = \frac{1}{4} \cdot \begin{bmatrix} 1 & 1 & 1 & 1 \\ \sqrt{3} & -1/\sqrt{3} & -1/\sqrt{3} & -1/\sqrt{3} \\ 0 & 2\sqrt{2/3} & -\sqrt{2/3} & -\sqrt{2/3} \\ 0 & 0 & \sqrt{2} & -\sqrt{2} \end{bmatrix} \tag{10}$$

It can be noted that the computation of the decoupling transformation does not depend on the angular displacements between the three-phase winding sets, thus overcoming the limitations of the VSD approach in terms of symmetrical and asymmetrical configurations (unless using numerical methods [28], [29]). For this reason, the decoupling transformation defined in (10) can be applied to any quadruple three-phase winding configuration, like the generic one shown in Fig. 4.

Therefore, by extension, the decoupling transformation defined in (9) can be applied to any multi-three-phase ac machine, regardless of the number n of three-phase winding sets and their angle displacements.

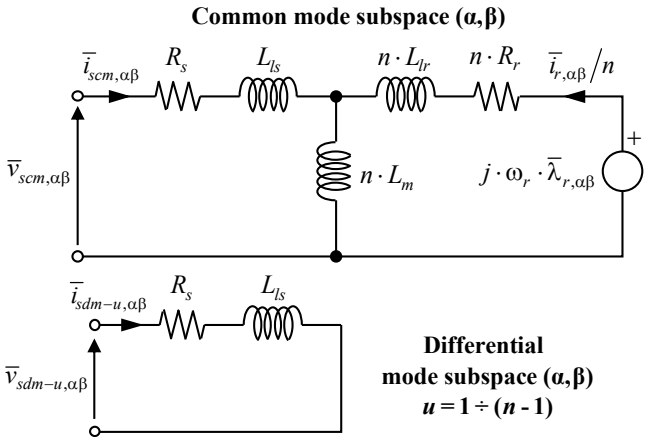

Fig. 5. Equivalent MS circuit of a multi-three-phase squirrel cage IM in stationary coordinates after the application of the decoupling transformation.

By merging (4) for all sets k=1÷n, the application of the decoupling transformation (8)-(9) leads to the redefinition of the MS machine model in the common-mode subspace as

$$\begin{cases} \bar{v}_{scm,xy} = R_s \cdot \bar{i}_{scm,xy} + \dfrac{d}{dt}\bar{\lambda}_{scm,xy} + j \cdot \omega_{xy} \cdot \bar{\lambda}_{scm,xy} \\ \bar{\lambda}_{scm,xy} = k_r \cdot \bar{\lambda}_{r,xy} + \left(L_{ls} + k_r \cdot n \cdot L_{lr}\right) \cdot \bar{i}_{scm,xy} \\ \bar{0} = \dfrac{\bar{\lambda}_{r,xy}}{\tau_r} + \dfrac{d}{dt}\bar{\lambda}_{r,xy} + j \cdot \omega_{slip} \cdot \bar{\lambda}_{r,xy} - k_r \cdot n \cdot R_r \cdot \bar{i}_{scm,xy} \end{cases} \tag{11}$$

The electromagnetic model of each differential subspace u (u=1÷(n-1)) is computed as:

$$\begin{cases} \bar{v}_{sdm-u,xy} = R_s \cdot \bar{i}_{sdm-u,xy} + \dfrac{d}{dt}\bar{\lambda}_{sdm-u,xy} + j \cdot \omega_{xy} \cdot \bar{\lambda}_{sdm-u,xy} \\ \bar{\lambda}_{sdm-u,xy} = L_{ls} \cdot \bar{i}_{sdm-u,xy} \end{cases} \tag{12}$$

Finally, the IM electromagnetic torque T is computed as:

$$T = \frac{3 \cdot n}{2} \cdot p \cdot \left(\bar{\lambda}_{scm,xy} \times \bar{i}_{scm,xy}\right) \tag{13}$$

According to (13), the electromagnetic torque is given by the cross product between the stator flux linkage vector and stator current vector, both belonging to the common-mode subspace since only there the interaction with the rotor is present. Therefore, the equivalent MS circuit of the IM after the application of the decoupling transformation is shown in Fig. 5. It can be noted that the magnetic couplings among the MS subspaces have been removed.

D. Differences between VSD and decoupled MS

Despite the resulting equation system (11)-(13) is similar to that obtained using the VSD approach (1)-(3), the mathematical/physical meaning of these two models is entirely different from each other. The VSD modeling performs a time-harmonic decoupling of the machine space [6]. Therefore, the energy conversion is represented just on average through the main subspace having the meaning of the time-fundamental model of the machine. Conversely, the common and differential models are computed through linear combinations of the MS variables. Therefore, the decoupling transformation performs its action on the time-fundamental subspaces of the machine, thus preserving the modularity of the energy conversion. By computing (9) for a dual three-phase machine, the resulting transformation matrix is similar to that defined in [19].

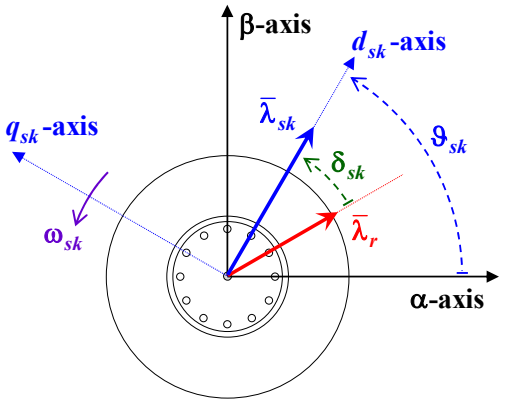

Fig. 6. Rotating stator flux frame (d_{sk},q_{sk}) of a generic three-phase unit k.

Therefore, the proposed decoupling method extends the results of [19] to multi-three-phase machines having an arbitrary number of three-phase sets, regardless if induction or synchronous machine is considered.

Finally, it can be noted that the main difference between the electromagnetic models of VSD harmonic-subspaces (2) and differential-modes subspaces (12) consists of the rotor equations. Indeed, the VSD approach models the rotor cage as an equivalent winding that emulates that of the stator, leading to the definition of harmonic and homopolar patterns also for it (last equation in (2)). However, these patterns are unnecessarily complicated and without a specific meaning. For this reason, the literature reports several variants of the VSD modeling [25] in which, like for the MS-approach, the rotor cage is considered as an equivalent three-phase winding, thus removing the patterns mentioned above. In this way, the decoupled MS model (11)-(13) and the VSD model (1)-(3) become formally identical to each other.

III. Control Scheme

In this work, the proposed decoupling method is used to implement a decoupled torque control of multi-three-phase IM drives. In detail, the decoupling transformation is implemented on the structure of an MS-based Direct Flux Vector Control scheme [12], [13].

The MS-based DFVC scheme is implemented in the rotating stator flux frame. According to the torque demand and operating speed, the MS-based DFVC aims at controlling n stator flux vectors and n stator current vectors in n stator flux frames (d_{sk}, q_{sk}, k=1÷n). Therefore, the position of the d_{sk}-axis corresponds with that of the k-unit stator flux vector ϑ_{sk}, as shown in Fig. 6. The load-angle δ_{sk} of each unit k is defined as the angular difference between the k-unit stator flux vector and the rotor flux vector. Finally, the angular speed of the k-unit stator flux vector ω_{sk} represents the synchronous speed of the rotating (d_{sk},q_{sk}) frame to the stationary (α,β) frame (Fig. 6).

The MS-based DFVC scheme can implement an independent regulation of both stator flux amplitude and torque contribution belonging to each three-phase unit [12]. This feature is useful when torque/power-sharing strategies between the units must be implemented [12], [25]–[27].

Nevertheless, when different operating conditions among the units are imposed, the load-angle values become different from each other. Therefore, it is not possible to identify a unique stator flux frame that is representative of all units. In the proposed control solution, this condition is not allowed. Indeed, because the control of both stator flux and torque is performed in common and differential subspaces, these can only be defined in a unique rotating frame.

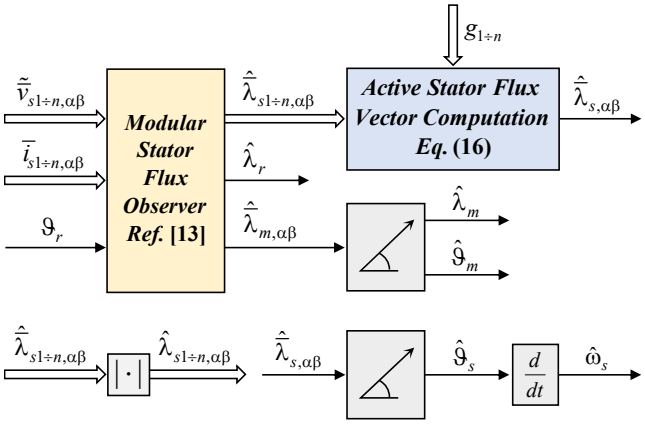

Fig. 7. Decoupled MS-based DFVC scheme: modular stator flux observer together with the computation of the rotating (d_s,q_s) frame in terms of angular position and synchronous speed.

For this reason, the decoupled torque control of the machine requires a balanced operation of the units, also corresponding to the most efficient operating condition of the drive. Therefore, the rotating frames of the healthy units must overlap, characterized by the same values of load-angle δ_s and synchronous speed ω_s. In this way, a unique stator flux frame (d_s,q_s) is identified.

A. Stator flux and torque equations

In the MS-based DFVC scheme, for each unit k, the stator flux amplitude λ_{sk} and q_{sk}-axis current component $i_{sk,q_{sk}}$ are controlled. According to (4), the k-unit stator electric equation along the d_{sk}-axis is computed as:

$$v_{sk,d_{sk}} = R_s \cdot i_{sk,d_{sk}} + \frac{d}{dt}\lambda_{sk} \tag{14}$$

Therefore, the regulation of the k-unit flux amplitude is performed by acting on the d_{sk}-axis voltage component $v_{sk,d_{sk}}$ of the k^{th} unit. Concerning the q_{sk}-axis current component, this can be considered as an equivalent torque-producing current. Indeed, by considering (5) in the rotating (d_{sk},q_{sk}) frame, the torque contribution T_k of k-unit is expressed as:

$$T_k = 3/2 \cdot p \cdot \lambda_{sk} \cdot i_{sk,q_{sk}} \tag{15}$$

In this work, the main goal is to demonstrate that the decoupling transformation can lead to a decoupled torque control of a multi-three-phase IM together with a straightforward reconfiguration of the control scheme after an open-three-phase fault event. Therefore, it follows a detailed description of the proposed control solution.

B. Stator flux observer

Because the MS-based DFVC scheme is implemented in stator flux (d_{sk},q_{sk}) coordinates, an observer is needed to estimate the flux vectors of all units in terms of amplitude $\hat{\lambda}_{sk}$ and angular position $\hat{\vartheta}_{sk}$ (superscript ˆ stands for observed variable). The proposed flux observer has a modular structure in which each unit k is considered regardless of the others. Further details regarding the observer design can be found in [13], [17], as they are beyond the goal of this work.

The outputs of the flux observer correspond to the stator flux vector of each unit k in stationary (α,β) coordinates $\hat{\bar{\lambda}}_{sk,\alpha\beta}$, the amplitude of the rotor flux vector $\hat{\lambda}_r$, and, the magnetizing flux vector in stationary (α,β) coordinates $\hat{\bar{\lambda}}_{m,\alpha\beta}$, as shown in Fig. 7. The definition of $\hat{\bar{\lambda}}_{m,\alpha\beta}$ is provided in the next subsections.

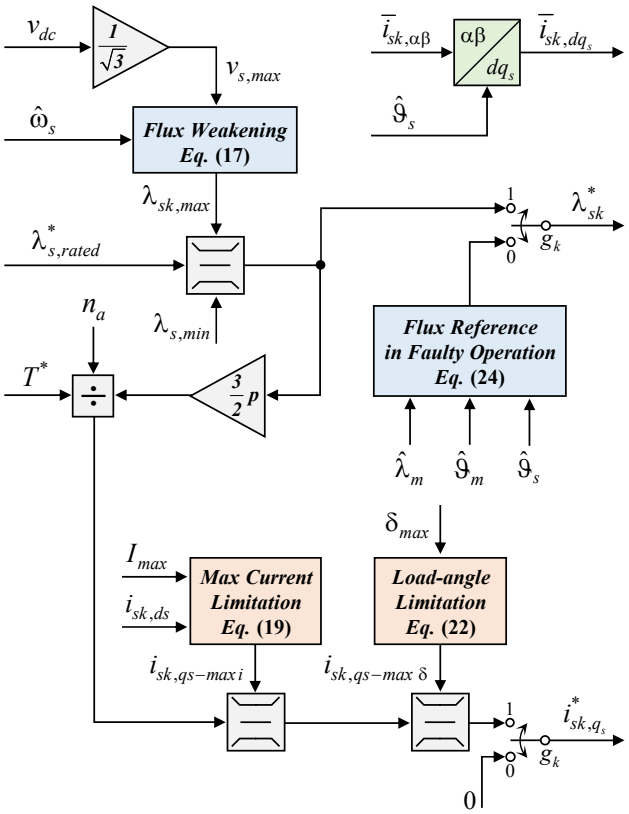

Fig. 8. Decoupled MS-based DFVC scheme: computation of the stator flux amplitude reference and torque-producing current reference for a generic unit *k*.

As previously reported, the decoupled MS-based DFVC scheme is implemented in the rotating (d_s,q_s) frame identified by the stator flux vectors of the healthy units. Therefore, an average vector that represents all operating units can be defined, using the following equation:

$$\hat{\bar{\lambda}}_{s,\alpha\beta} = \frac{\sum_{k=1}^{n}\left(g_k \cdot \hat{\bar{\lambda}}_{sk,\alpha\beta}\right)}{\sum_{k=1}^{n} g_k} = \frac{1}{n_a}\cdot\sum_{k=1}^{n}\left(g_k \cdot \hat{\bar{\lambda}}_{sk,\alpha\beta}\right) \qquad (16)$$

where g_k represents the status of the considered unit k (0=*faulty*, 1=*healthy*) while n_a is the number of healthy units. Finally, from the average stator flux vector defined in stationary (α,β) coordinates (16), the computation of both d_s-axis angular position ϑ_s and synchronous speed of the rotating (d_s,q_s) frame is performed, as shown in Fig. 7.

C. Stator flux amplitude reference and torque-producing current reference for the healthy units

According to the MS-based DFVC scheme [13], [17], the primary inputs of the control structure dedicated to each healthy unit k, are the following (Fig. 8):

- Torque reference T^*, usually provided by an external control loop that depends on the drive application;
- Phase-current amplitude limit $I_{\max}$, usually related to the current limit of the inverter and/or the machine;
- Load-angle limit δ_{max} (the same limit for all the units);
- DC-link voltage v_{dc}.

Below the base speed, the flux amplitude reference of each healthy unit k is set to the rated value $\lambda_{s,rated}$, as shown in Fig. 8.

If the inverter voltage limit $v_{s,max}$ is reached ($v_{dc}/\sqrt{3}$), the flux amplitude references of the healthy units are limited to allow the drive operation under the voltage constraint. According to the MS electromagnetic model (4), computed in the rotating (d_s,q_s) frame, the stator flux limit $\lambda_{sk,max}$ of each healthy unit k is computed as:

$$\lambda_{sk,max} \le \frac{\sqrt{v_{s,\max}^2 - \left(\tilde{R}_s \cdot i_{sk,ds}\right)^2} - \tilde{R}_s \cdot i_{sk,qs} \cdot sign\left(\hat{\omega}_s\right)}{\left|\hat{\omega}_s\right|} \qquad (17)$$

where the superscript ~ stands for estimated variable and/or parameter. As shown in Fig. 8, the components of the k-unit stator current vector in the rotating (d_s,q_s) frame are computed by applying the conventional rotational transformation [24] on the k-unit stator current vector defined in stationary (α,β) coordinates, using the d_s-axis angular position ϑ_s as angle reference.

Since the reference frames of the healthy units overlap, in (17), the synchronous speed of the rotating (d_s,q_s) frame ω_s has been used, as shown in Fig. 8. Therefore, a single synchronous speed is computed for all the units (Fig. 7), using a conventional phase-locked loop [30]. It can be noted that (17) leads to a straightforward flux-weakening regulation law without the use of any voltage/flux regulators (as with the MS-based FOC schemes).

Finally, the stator flux amplitude reference of each unit k λ_{sk}^* is limited at the minimum value $\lambda_{s,min}$, as shown in Fig. 8. This limit is lower than the minimum value required at the flux-weakening operation, with the maximum motor speed and the minimum DC-link voltage.

Since a balanced machine operation is considered, the machine torque reference T^* is shared equally between the healthy units. Therefore, by using (15), the q_s-axis current reference of each healthy unit k is computed as:

$$i_{sk,q_s}^* = \frac{2}{3\cdot p\cdot \lambda_{sk}^*}\cdot T_k^* = \frac{2}{3\cdot p\cdot \lambda_{sk}^*}\cdot\frac{T^*}{n_a} \qquad (18)$$

The torque-producing current reference (18) of each unit k is subjected to two consecutive limitations, corresponding to the constraints of maximum phase-current amplitude I_{max} and maximum load-angle δ_{max}, a shown in Fig. 8.

The first saturation limit $i_{sk,qs\text{-}max\,i}$ does not depend on the torque sign but only on the current limit $I_{\max}$ as follows:

$$\left|i_{sk,qs}^*\right| \le i_{sk,qs-max\,i} = \sqrt{I_{max}^2 - i_{sk,ds}^2} \qquad (19)$$

Regarding the k-unit load-angle limitation, the stator magnetic equation (4) computed in (d_{sk},q_{sk}) coordinates is considered:

$$\bar{\lambda}_{sk,dq_{sk}} = k_r\cdot\bar{\lambda}_{r,dq_{sk}} + L_{ls}\cdot\bar{i}_{sk,dq_{sk}} + k_r\cdot L_{lr}\cdot\sum_{l=1}^{n}\bar{i}_{sl,dq_{sk}} \qquad (20)$$

Since the balanced operation of the healthy units is considered, (20) can be referred to the rotating (d_s,q_s) frame as follows:

$$\bar{\lambda}_{sk,dq_s} = k_r\cdot\bar{\lambda}_{r,dq_s} + L_{ls}\cdot\bar{i}_{sk,dq_s} + n_a\cdot k_r\cdot L_{lr}\cdot\bar{i}_{sk,dq_s} \qquad (21)$$

To highlight the relationship between the k-unit stator magnetic equation (21) and the k-unit load-angle δ_{sk}, the vector diagram is shown in Fig. 9. According to it, the implementation of the k-unit load-angle limitation leads to the definition of the saturation limit $i_{sk,qs\text{-}max\ \delta}$. This is applied regardless of the k-unit torque-producing current reference, leading to the regulation law (22).

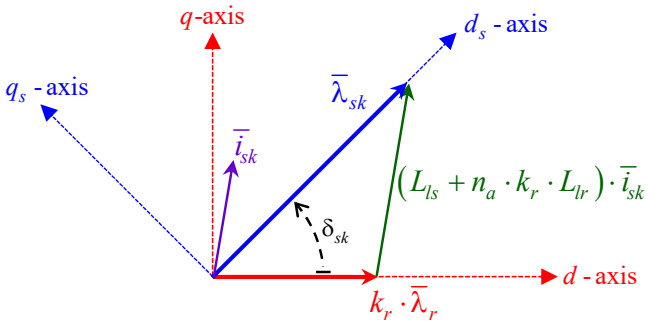

Fig. 9. Vector diagram representing the k-unit stator magnetic model for the balanced operation of the healthy units.

$$\left|i^{*}_{sk,qs}\right| \le i_{sk,qs-max\ \delta} = \frac{\tilde{k}_r \cdot \hat{\lambda}_r}{\tilde{L}_{ls} + n_a \cdot \tilde{k}_r \cdot \tilde{L}_{lr}} \cdot \sin\left(\delta_{max}\right) \quad (22)$$

It can be noted how the k-unit load-angle limitation is performed without the use of any external controller [16], leading to a model-based regulation law that avoids demanding tuning procedures. According to [17], [24], the load-angle limit that avoids pull-out corresponds at 45 electrical degrees, thus performing the MTPV operation.

D. Stator flux amplitude reference and torque-producing current reference for the faulty units

If an open-three-phase fault event occurs, the stator flux of the faulty unit k corresponds to the magnetizing flux of the machine. Therefore, according to (4), this is computed as:

$$\bar{\lambda}_{m,\alpha\beta} = k_r \cdot \bar{\lambda}_{r,\alpha\beta} + k_r \cdot L_{lr} \cdot \sum_{l=1,l\neq k}^{n} \bar{i}_{sl,\alpha\beta} \quad (23)$$

The magnetizing flux components in stationary (α,β) frame can be estimated using the flux observer belonging to the MS-based DFVC scheme [13], as shown in Fig. 7. Therefore, by denoting with $\hat{\lambda}_m$ and $\hat{\vartheta}_m$ the observed amplitude and angular position of the magnetizing flux vector respectively, the flux reference of the faulty unit k is computed in the rotating (d_s,q_s) frame as:

$$\lambda^{*}_{sk} = \hat{\lambda}_m \cdot \cos\left(\hat{\vartheta}_s - \hat{\vartheta}_m\right) \quad (24)$$

Regarding the k-unit torque-producing current reference, this must be set at zero (Fig. 8):

$$i^{*}_{sk,q_s} = 0 \quad (25)$$

In conclusion, based on the k-unit status g_k, the stator flux amplitude reference and the torque-producing current reference of the unit k are appropriately set, according to the control scheme shown in Fig. 8.

E. Conventional MS-based DFVC scheme

In the conventional MS-based DFVC scheme, no decoupling actions are performed [14], [31]. Therefore, once the references of the generic unit k are computed (Fig. 8), the k-unit torque control is directly performed, as shown in Fig. 10.

The main advantage of this approach is its simplicity, as no decoupling actions are needed, and the implementation of complex control algorithms is avoided [12], [13].

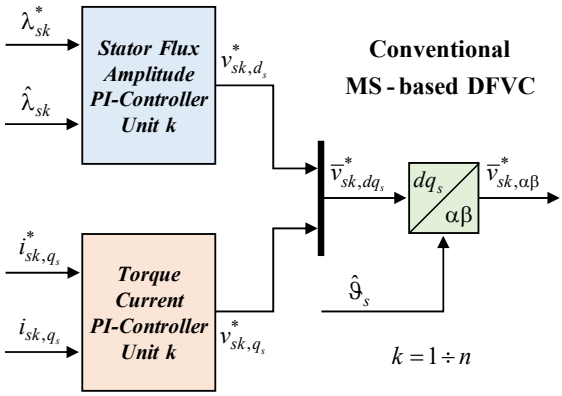

Fig. 10. Conventional MS-based DFVC scheme: regulation of the stator flux amplitude and torque-producing current for a generic unit k.

Another advantage is the possibility to implement an unbalanced torque- and flux- sharing operation among the units [12], [27], thus obtaining more degrees of freedom than the proposed control solution.

However, the conventional MS-based DFVC may present instability phenomena, especially in the case of multi-three-phase machines having more than two three-phase sets. Although the d_{sk}-axes (flux) are decoupled, as shown in (14), the q_{sk}-axes (torque) are coupled because the q_{sk}-axis voltage component of each unit k also contributes to the control of the torque-producing currents of the other units [12], [17]. Therefore, without any decoupling actions of the q_{sk}-axes, the Proportional-Integral (PI) controllers performing the control of the torque-producing currents of the machine act in conflict with each other and may cause the instability of the control scheme. The lack of a decoupling action is possible if the bandwidth of the torque controllers is lowered, resulting in lower quality of the phase-currents [31].

When FOC schemes are employed, the risk of instability is much higher with respect to the DFVC since both (d,q) control axes require proper decoupling. A proof of this statement has been provided in [18], where the authors reported the instability of the MS-based FOC scheme for a dual three-phase permanent magnet machine.

Regardless of the number of the three-phase units, the proposed control solution solves all the issues mentioned above, as demonstrated in the next subsections.

F. Application of the decoupling transformation

The proposed control scheme performs the regulation of the stator flux amplitude and torque-producing current of each unit k in terms of common and differential modes, as shown in Fig. 11. Therefore, by considering both references and observed values of the stator fluxes amplitudes of the units (λ^{*}_{sk} - $\hat{\lambda}_{sk}$, k=1÷n), their corresponding values in terms of common and differential modes are computed as:

$$\begin{Bmatrix} \lambda^{*}_{scm} \\ \lambda^{*}_{sdm-1} \\ \dots \\ \lambda^{*}_{sdm-(n-1)} \end{Bmatrix} = [T_d] \cdot \begin{Bmatrix} \lambda^{*}_{s1} \\ \lambda^{*}_{s2} \\ \dots \\ \lambda^{*}_{sn} \end{Bmatrix} ; \begin{Bmatrix} \hat{\lambda}_{scm} \\ \hat{\lambda}_{sdm-1} \\ \dots \\ \hat{\lambda}_{sdm-(n-1)} \end{Bmatrix} = [T_d] \cdot \begin{Bmatrix} \hat{\lambda}_{s1} \\ \hat{\lambda}_{s2} \\ \dots \\ \hat{\lambda}_{sn} \end{Bmatrix} \quad (26)$$

Similarly, the reference and measured values of the torque-producing currents of the units (i^{*}_{sk,q_s} - i_{sk,q_s} , k=1÷n) are computed in terms of common and differential values (27).

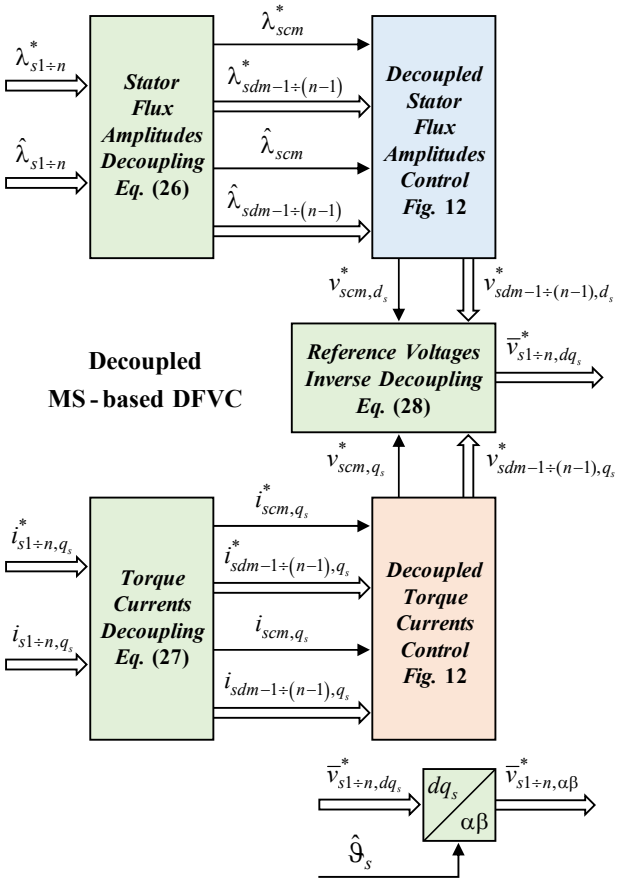

Fig. 11. Decoupled MS-based DFVC scheme: application of the decoupling transformation.

$$\begin{Bmatrix} i^*_{scm,q_s} \\ i^*_{sdm-1,q_s} \\ \cdots \\ i^*_{sdm-(n-1),q_s} \end{Bmatrix} = [T_d] \cdot \begin{Bmatrix} i^*_{s1,q_s} \\ i^*_{s2,q_s} \\ \cdots \\ i^*_{sn,q_s} \end{Bmatrix}; \begin{Bmatrix} i_{scm,q_s} \\ i_{sdm-1,q_s} \\ \cdots \\ i_{sdm-(n-1),q_s} \end{Bmatrix} = [T_d] \cdot \begin{Bmatrix} i_{s1,q_s} \\ i_{s2,q_s} \\ \cdots \\ i_{sn,q_s} \end{Bmatrix} \tag{27}$$

The application of (26)-(27) does not correspond to the definition given in (8), defined for the vector variables. However, it can be applied component by component without any issue. Therefore, two parallel scalar controls are implemented for the control of the common and differential components of the stator flux amplitude and torque producing current.

It is highlighted that the computation of the common-mode and differential-mode references is not affected by open-three-phase fault events. In this case, it is only necessary to redefine the references of the faulty unit using (24)-(25), as shown in Fig. 8. This is further proof that the proposed control scheme behaves like a VSD-based one while keeping the modularity since it is implemented on the structure of an MS-based DFVC scheme.

G. Decoupled torque control

Once the reference and feedback signals are computed in terms of common and differential values, the decoupled torque control of the machine is performed, as shown in Fig. 12. For each subspace, a couple of PI controllers are employed, one for the common/differential flux amplitude regulation and one for the common/differential torque current regulation.

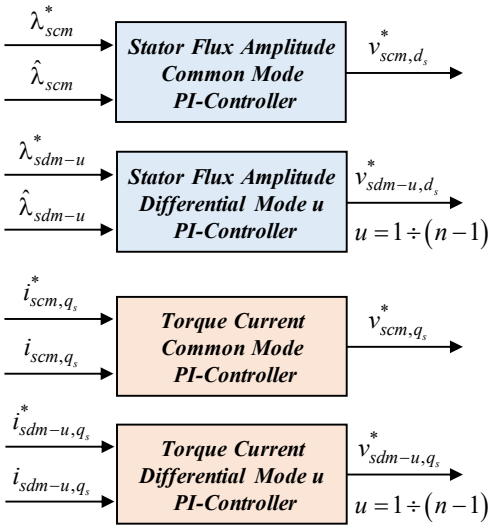

Fig. 12. Decoupled MS-based DFVC scheme: regulation of the common and differential modes of the stator flux amplitude and torque-producing current.

The control of the common-mode subspace is responsible for the energy conversion, thus having the same meaning as the VSD main subspace. Conversely, the control of the differential subspaces is performed to manage any possible unbalances among the sets in terms of flux and torque production, thus having a similar behavior to the VSD harmonic subspaces. Besides, because the equation system of the common and differential subspaces (11)-(13) is formally identical to that of the VSD subspaces (1)-(3), the design of the PI controllers can be performed using the same procedure defined for the VSD-based control schemes.

The outputs of the PI controllers are the common $\overline{v}^*_{scm,dq_s}$ and differential $\overline{v}^*_{sdm-u,dq_s}$ (u=1÷(n-1)) stator voltage vector references. Therefore, to obtain the voltage vector references of the units $\overline{v}^*_{sk,dq_s}$ (k=1÷n) in the rotating (d_s,q_s) frame, the inverse decoupling transformation is applied (Fig. 11):

$$\begin{Bmatrix} \overline{v}^*_{s1,dq_s} \\ \overline{v}^*_{s2,dq_s} \\ \cdots \\ \overline{v}^*_{sn,dq_s} \end{Bmatrix} = [T_d]^{-1} \cdot \begin{Bmatrix} \overline{v}^*_{scm,dq_s} \\ \overline{v}^*_{sdm-1,dq_s} \\ \cdots \\ \overline{v}^*_{sdm-(n-1),dq_s} \end{Bmatrix} \tag{28}$$

Once the (d_s,q_s) voltage references of the units are computed, they are referred to the stationary (α,β) frame by using the inverse rotation transformation, as shown in Fig. 11. Finally, according to the MS-based DFVC scheme [12]–[14], the computation of the inverter commands of each unit is performed [12]. Further details about the Pulse-Width Modulation (PWM) control of the three-phase units can be found in [12]–[14], as they are beyond the scope of this work.

IV. Experimental Validation

The machine used for the experimental validation is a 12-phase asymmetrical IM prototype having four three-phase winding sets shifted by 15 electrical degrees (full-pitch windings with one slot/pole/phase), as shown in Fig. 13.

The main features of the machine under test are reported in Table I [32].

TABLE I. CHARACTERISTICS OF THE MACHINE UNDER TEST

Main Data	
Phase Number	12 (4x3-phase)
Pole number	4
Rated power	10 kW
Rated speed	6000 rpm
Rated phase-voltage	115 V (rms)
Rated phase-current	10 A (rms)
Machine Parameters @ 25°C	
Stator resistance R_s	145 mΩ
Stator leakage inductance L_{ls}	0.94 mH
Magnetizing inductance L_m	4.3 mH
Rotor resistance R_r	45 mΩ
Rotor leakage inductance L_{lr}	0.235 mH
Rated stator flux amplitude $\lambda_{s,rated}$	0.115 Vs

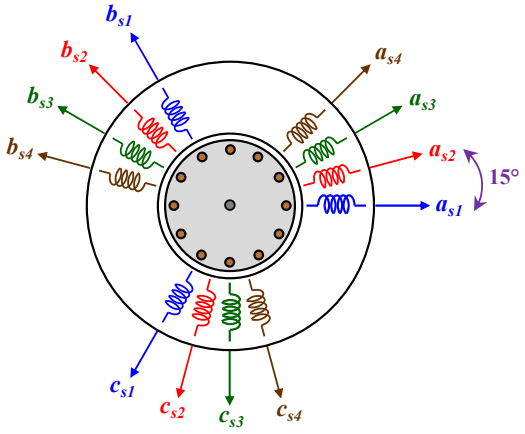

Fig. 13. Asymmetrical 12-phase IM using a quadruple three-phase stator winding configuration.

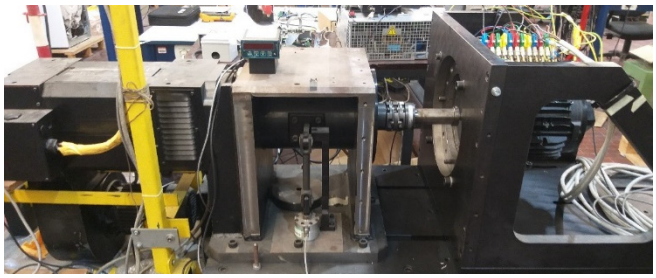

Fig. 14. View of the machine under test (right) and the driving machine (left).

A. Test rig

The machine has been mounted on a test rig for development purposes. The rotor shaft has been coupled to a driving machine acting as an active mechanical load, as shown in Fig. 14. Due to the mechanical limitations of the test rig, the maximum speed has been limited at ±6000 rpm. The mechanical rotor position has been measured with an incremental encoder using 1024 pulses/rev.

The power converter consists of four independent three-phase IGBT power modules (100 A, 1200 V) fed at 270 V [33]. The switching frequency has been set at 5 kHz, such as to be compatible with the industrial implementations. The dead-time of the inverter units has been set at 1.5 µs.

The digital controller is the dSPACE® DS1103 PPC Controller Board, using 5 kHz of sampling frequency (single-edge PWM modulation), while the control algorithm has been developed in the C-code environment.

The experimental results are provided for the drive operation with torque control mode and speed control mode.

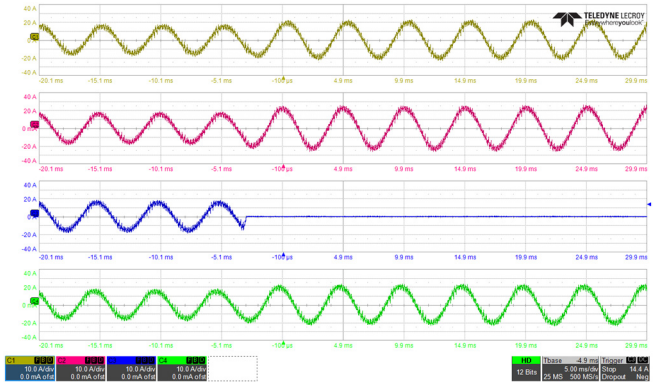

Fig. 15. Inverter 3 shut-off in generation mode (-6000 rpm, 16 Nm). Ch1: i_{as1} (10 A/div), Ch2: i_{as2} (10 A/div), Ch3: i_{as3} (10 A/div), Ch4: i_{as4} (10 A/div). Time resolution: 5 ms/div.

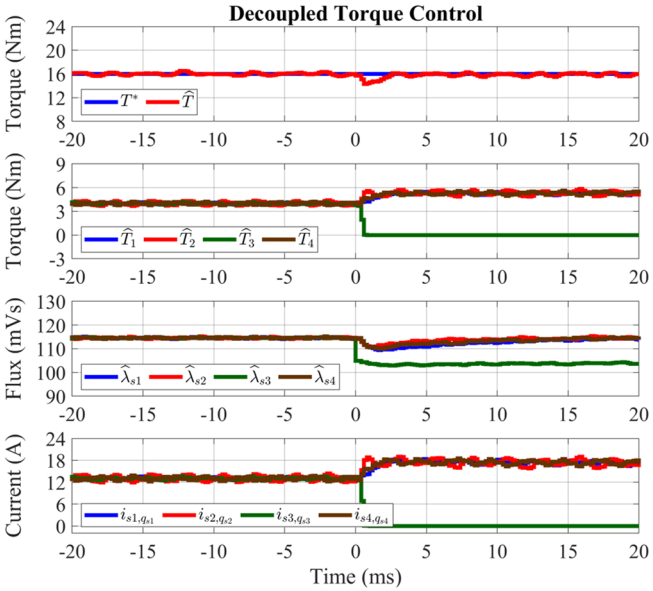

Fig. 16. Inverter 3 shut-off (at t=0) in generation mode (-6000 rpm, 16 Nm). From top to bottom: reference and observed torque (Nm); observed single units torque (Nm), observed single units stator flux amplitude (mVs); measured single units torque-producing current (A).

B. Experimental results in Torque Control Mode

The open-loop torque control operation has been performed with the driving machine acting as the prime mover (speed controlled). The fault-tolerance capability of the drive has been tested. Starting from rated generating conditions (-6000 rpm, 16 Nm), the inverter power module 3 has suddenly been turned off. A fault of a power module can cause this event. The experimental results are shown in Figs. 15-18.

Fig. 15 shows the waveforms of phase-currents $i_{as1\div4}$ before and after the fault event. Compared to the results obtained with the conventional MS-based DFVC scheme [31], the phase-currents are less distorted due to the effectiveness of the proposed decoupling transformation.

Since the currents of the healthy units must increase to keep the same torque and machine flux (Fig. 15), the control of the common-mode subspace is little affected by the fault event, as shown in Figs. 17-18. Conversely, the variables in the differential subspaces depend on the unbalances among the three-phase units in terms of flux and torque productions.

Before the fault event, the units were having a balanced operation. Therefore, the currents and fluxes of the differential mode subspaces have been controlled at zero value, as shown in Figs. 17-18. After the fault event, the flux and torque contributions of the third unit are missing, thus leading to a strong unbalance among the healthy units and the faulty one.

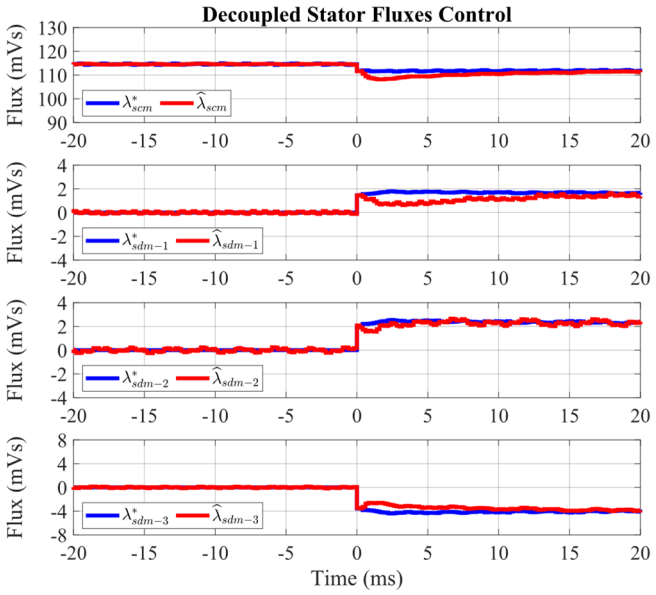

Fig. 17. Inverter 3 shut-off (at t=0) in generation mode (-6000 rpm, 16 Nm). Common and differential subspaces control of the stator fluxes amplitude (mVs) of the units.

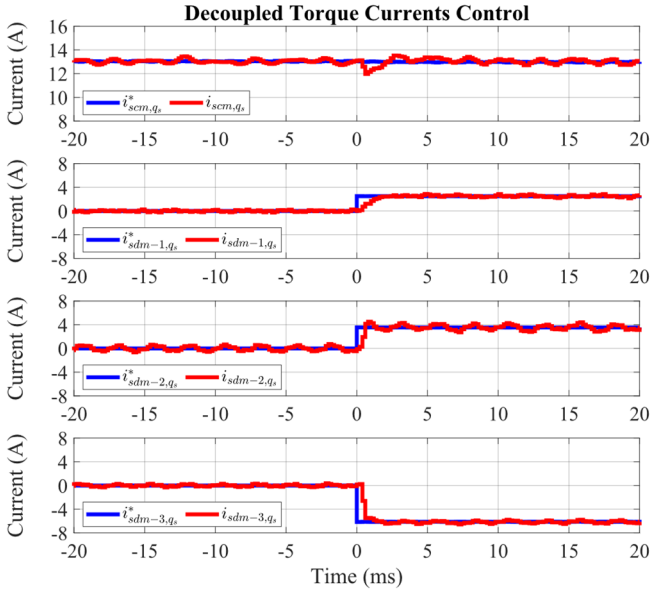

Fig. 18. Inverter 3 shut-off (at t=0) in generation mode (-6000 rpm, 16 Nm). Common and differential subspaces control of the torque-producing current (A) of the units.

Therefore, to keep balanced the waveforms of the healthy units (currents, fluxes), the differential mode subspaces have been properly controlled (Figs. 17-18).

At steady-state, the differential subspaces variables are dc quantities, thus allowing the use of conventional PI controllers. Finally, due to machine asymmetries related to the second winding set (Fig. 16), the torque-producing current component belonging to the second differential subspace is characterized by slight disturbances. However, the phase-currents of the healthy units are not affected by them since they exhibit a sinusoidal waveform, as shown in Fig. 15.

The work also focuses on the torque performance when one or more units are turned off. For example, a fast torque-transient (10 Nm/ms) from no-load up to the rated generating conditions (16 Nm, -6000 rpm), with unit 3 turned off, is described in Figs. 19-22.

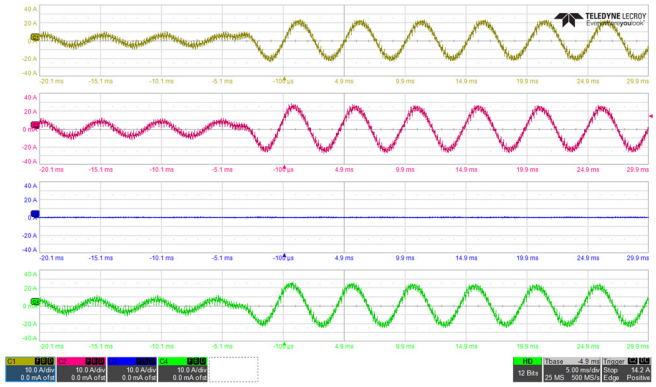

Fig. 19. Fast torque transient (10 Nm/ms) from no-load up to rated torque (16 Nm) in generation mode at -6000 rpm with unit 3 turned off. Ch1: i_{as1} (10 A/div), Ch2: i_{as2} (10 A/div), Ch3: i_{as3} (10 A/div), Ch4: i_{as4} (10 A/div). Time resolution: 5 ms/div.

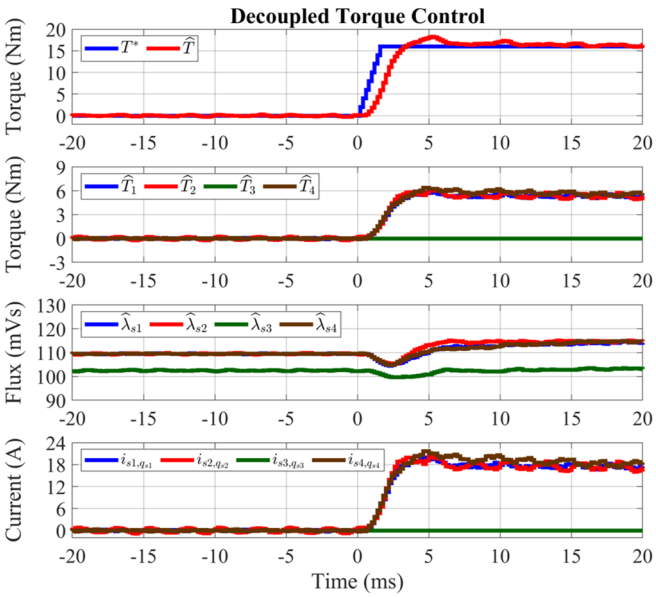

Fig. 20. Fast torque transient (10 Nm/ms) from no-load up to rated torque (16 Nm) in generation mode at -6000 rpm with unit 3 turned off. From top to bottom: reference and observed torque (Nm); observed single units torque (Nm), observed single units stator flux amplitude (mVs); measured single units torque-producing current (A).

Fig. 19 shows the waveforms of phase-currents $i_{as1\div4}$ during the torque transient. It is noted that the currents of the healthy units are perfectly sinusoidal also in no-load conditions.

Because unit 3 was turned off, the common and differential subspaces have adequately been controlled in both no-load and rated torque conditions, as shown in Fig. 21-22. In detail, the steady-state values of both MS variables (Fig. 20) and common/differential mode variables (Figs. 21-22) correspond to those obtained in the previous test after unit 3 shuts off.

It is noted that, for each healthy unit, the reference values of flux amplitude and torque-producing current have been imposed without a significant overshoot and with an excellent dynamic response.

Finally, since the flux amplitude reference of unit 3 is computed through (24), the control of the common and differential subspaces in terms of fluxes amplitudes is slightly affected by the dynamics of the flux observer.

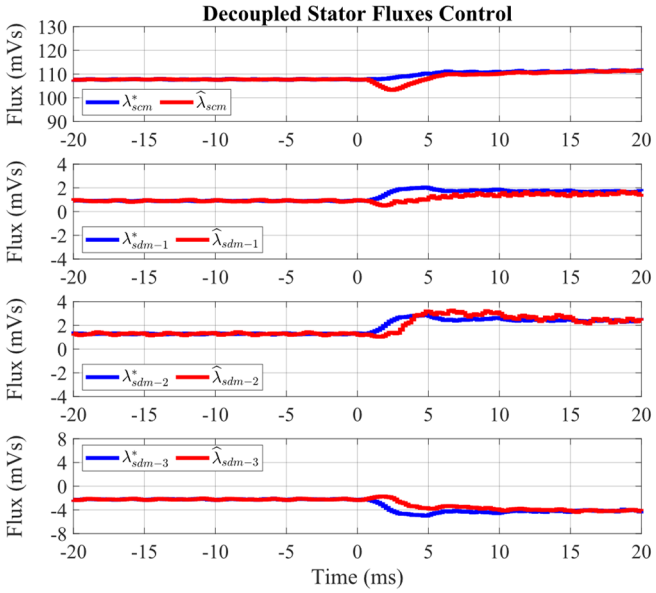

Fig. 21. Fast torque transient (10 Nm/ms) from no-load up to rated torque (16 Nm) in generation mode at -6000 rpm with unit 3 turned off. Common and differential subspaces control of the stator fluxes amplitude (mVs) of the units.

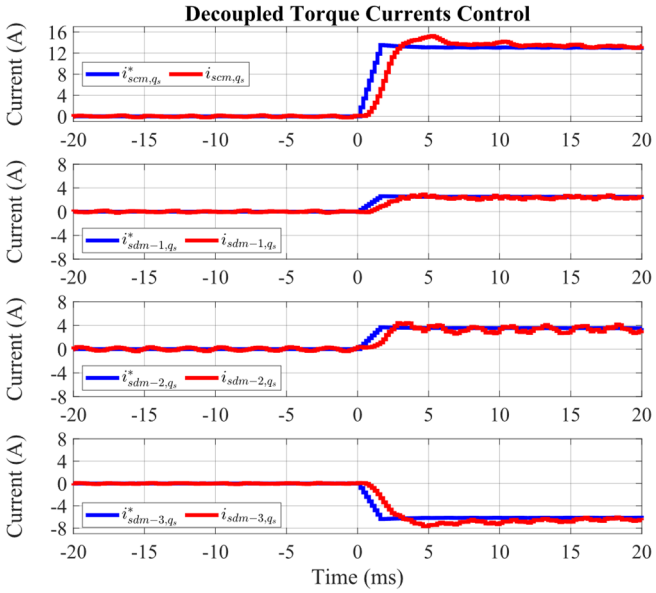

Fig. 22. Fast torque transient (10 Nm/ms) from no-load up to rated torque (16 Nm) in generation mode at -6000 rpm with unit 3 turned off. Common and differential subspaces control of the torque-producing current (A) of the units.

In terms of common and differential modes, the references of the fluxes amplitudes do not correspond to a ramp (Fig. 21). Conversely, since the reference of the torque-producing current of unit 3 is directly set at zero according to (25), the common and differential mode references of the torque-producing currents, follow a profile similar to that of the torque reference (Fig. 22).

In conclusion, this test proves the effectiveness of the proposed decoupling solution in dynamic torque conditions.

C. *Experimental results in Speed Control Mode*

To test the flux-weakening with MTPV operation below the base speed of the machine (near to 6000 rpm), the DC-link voltage has been reduced from 270 V to 135 V.

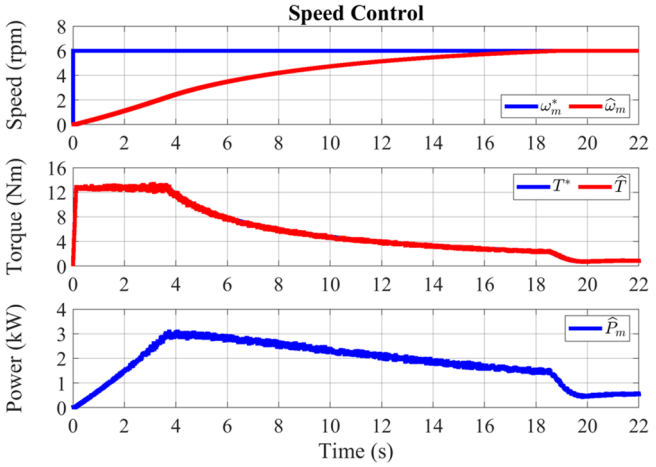

Fig. 23. Speed control with inertial load from 0 to 6000 rpm. From top to bottom: reference and estimated speed (krpm); reference and observed total torque (Nm); estimated mechanical power (kW).

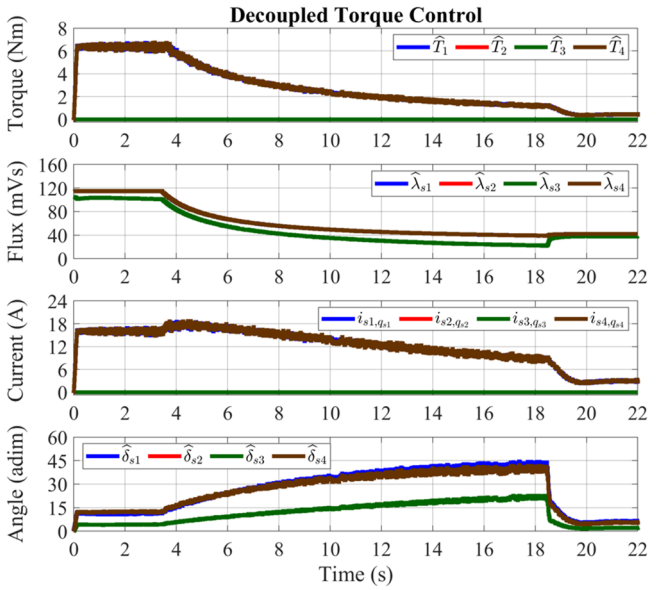

Fig. 24. Speed control with inertial load from 0 to 6000 rpm. From top to bottom: observed single units torque (Nm), observed single units stator flux amplitude (mVs); measured single units torque-producing current (A), observed single units load-angle (deg).

The closed-loop speed control operation has been tested with the driving machine acting as an inertial load. The speed control has been implemented with a simple PI controller whose output is the reference torque provided to the decoupled MS-based DFVC scheme.

Two units have been turned off (units 2 and 3). In this way, the control performance of the differential modes has been tested under the inverter voltage and current constraints. The obtained results for a step reference from 0 up to 6000 rpm are shown in Figs. 23-26.

It is noted how, without any voltage limitation, the torque is limited only by the power converter current limit (I_{max} = 24 A). The flux-weakening becomes active for a speed that is near to 2500 rpm. The torque reduction is approximately proportional to the increment of the speed [34]. It is noted how the flux amplitudes and the stator currents of the healthy units are properly controlled, as shown in Fig. 24. The MTPV operation starts when the load-angles of the healthy units become properly limited at 45 electrical degrees, at a speed of about 5500 rpm.

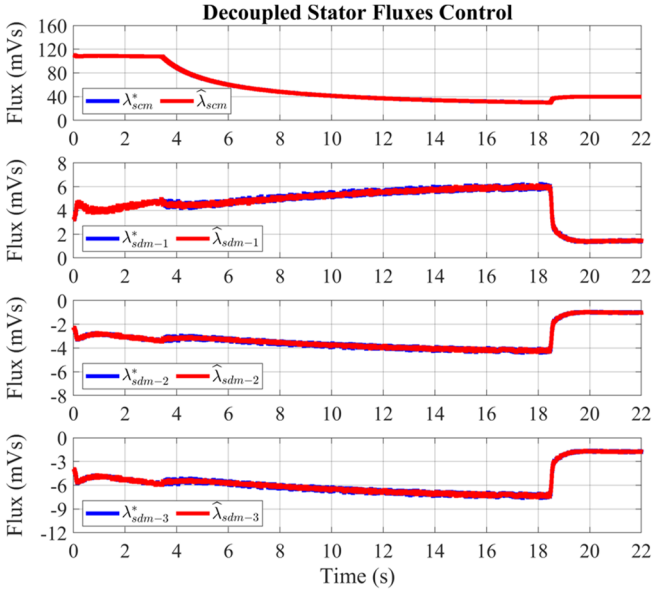

Fig. 25. Speed control with inertial load from 0 to 6000 rpm. Common and differential subspaces control of the stator fluxes amplitude (mVs) of the units.

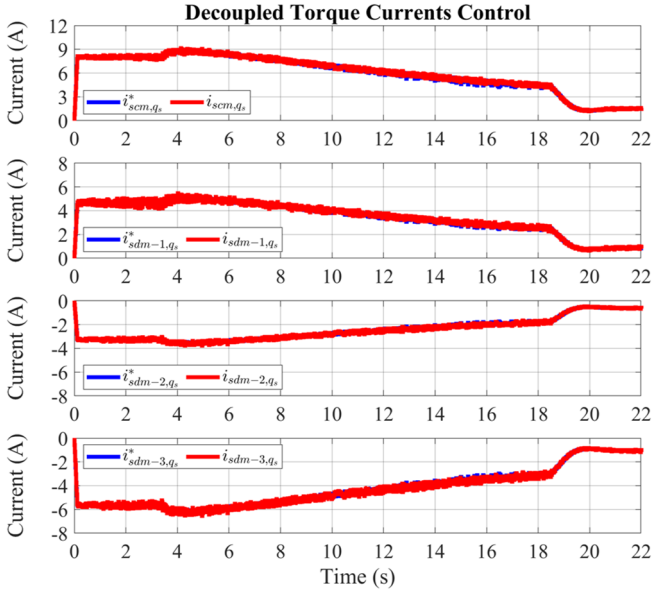

Fig. 26. Speed control with inertial load from 0 to 6000 rpm. Common and differential subspaces control of the torque-producing current (A) of the units.

Due to the strong unbalance among the healthy units and the faulty ones in terms of flux and torque production, the active control of the differential subspaces is performed, as shown in Figs. 25-26. It can be noted that the profiles of differential-mode flux amplitudes and differential-mode torque-producing currents are similar to those encountered in the common subspace. Besides, as with the test shown in Fig. 17, some differential-mode flux amplitudes are controlled at negative values. However, the differential-mode variables have only a mathematical meaning. Therefore, no physical law is violated.

In conclusion, the experimental results demonstrate that the proposed solution allows a decoupled torque control of a multi-three-phase IM together with a straightforward reconfiguration of the control scheme after an open-three-phase fault event, thus combining the advantages of the VSD-based and MS-based control schemes.

V. Conclusion

The paper proposes a new decoupling transformation able to remove the electromagnetic couplings among the units of a multi-three-phase machine controlled with the multi-stator (MS) approach. To implement a decoupled torque control of multi-three-phase induction motor (IM) drives, the proposed decoupling method has been applied to a modular MS-based, direct flux vector control (DFVC) scheme.

The performance of the proposed control solution has been validated with a twelve-phase IM prototype using a quadruple three-phase winding configuration. The experimental results demonstrate the feasibility of the proposed control solution both in healthy and faulty operation (open-winding fault events), as well as in deep flux-weakening with maximum torque per voltage (MTPV) operation. The advantages of the proposed decoupling method can be summarized as follows:

- Machine model similar to that computed using the VSD approach, preserving the modularity of the MS modeling and requiring the application of a reference transformation easy to implement.
- Possibility of applying the decoupling transformation on any multi-three-phase machine, overcoming the VSD limits in terms of symmetrical/asymmetrical configurations.
- Computation of the reference variables (currents, fluxes) starting from those computed using the MS modeling, allowing easy reconfiguration of the control scheme after an open-three-phase fault event.

References

[1] R. Bojoi, S. Rubino, A. Tenconi, and S. Vaschetto, 'Multiphase electrical machines and drives: A viable solution for energy generation and transportation electrification', in *2016 International Conference and Exposition on Electrical and Power Engineering (EPE)*, 2016, pp. 632–639, doi: 10.1109/ICEPE.2016.7781416.

[2] W. Cao, B. C. Mecrow, G. J. Atkinson, J. W. Bennett, and D. J. Atkinson, 'Overview of Electric Motor Technologies Used for More Electric Aircraft (MEA)', *IEEE Trans. Ind. Electron.*, vol. 59, no. 9, pp. 3523–3531, Sep. 2012, doi: 10.1109/TIE.2011.2165453.

[3] E. Jung, H. Yoo, S. Sul, H. Choi, and Y. Choi, 'A Nine-Phase Permanent-Magnet Motor Drive System for an Ultrahigh-Speed Elevator', *IEEE Trans. Ind. Appl.*, vol. 48, no. 3, pp. 987–995, May 2012, doi: 10.1109/TIA.2012.2190472.

[4] 'EAIR - Electromobility - Siemens'. [Online]. Available: http://w3.siemens.com/topics/global/en/electromobility/pages/eair.aspx. [Accessed: 10-Nov-2019].

[5] 'The leader in renewable energy I Siemens Gamesa'. [Online]. Available: https://www.siemensgamesa.com/en-int. [Accessed: 10-Nov-2019].

[6] Y. Zhao and T. A. Lipo, 'Space vector PWM control of dual three-phase induction machine using vector space decomposition', *IEEE Trans. Ind. Appl.*, vol. 31, no. 5, pp. 1100–1109, Sep. 1995, doi: 10.1109/28.464525.

[7] E. Levi, R. Bojoi, F. Profumo, H. A. Toliyat, and S. Williamson, 'Multiphase induction motor drives - a technology status review', *IET Electr. Power Appl.*, vol. 1, no. 4, pp. 489–516, Jul. 2007, doi: 10.1049/iet-epa:20060342.

[8] E. Levi, 'Multiphase Electric Machines for Variable-Speed Applications', *IEEE Trans. Ind. Electron.*, vol. 55, no. 5, pp. 1893–1909, May 2008, doi: 10.1109/TIE.2008.918488.

[9] L. Zheng, J. E. Fletcher, B. W. Williams, and X. He, 'A Novel Direct Torque Control Scheme for a Sensorless Five-Phase Induction Motor Drive', *IEEE Trans. Ind. Electron.*, vol. 58, no. 2, pp. 503–513, Feb. 2011, doi: 10.1109/TIE.2010.2047830.

[10] J. K. Pandit, M. V. Aware, R. V. Nemade, and E. Levi, 'Direct Torque Control Scheme for a Six-Phase Induction Motor With Reduced Torque Ripple', *IEEE Trans. Power Electron.*, vol. 32, no. 9, pp. 7118–7129, Sep. 2017, doi: 10.1109/TPEL.2016.2624149.

[11] R. H. Nelson and P. C. Krause, 'Induction Machine Analysis for Arbitrary Displacement Between Multiple Winding Sets', *IEEE Trans. Power Appar. Syst.*, vol. PAS-93, no. 3, pp. 841–848, May 1974, doi: 10.1109/TPAS.1974.293983.

[12] S. Rubino, R. Bojoi, F. Mandrile, and E. Armando, 'Modular Stator Flux and Torque Control of Multiphase Induction Motor Drives', in *2019 IEEE International Electric Machines and Drives Conference (IEMDC)*, 2019, pp. 531–538, doi: 10.1109/IEMDC.2019.8785376.

[13] S. Rubino, R. Bojoi, S. A. Odhano, and P. Zanchetta, 'Model Predictive Direct Flux Vector Control of Multi-three-Phase Induction Motor Drives', *IEEE Trans. Ind. Appl.*, vol. 54, no. 5, pp. 4394–4404, Sep. 2018, doi: 10.1109/TIA.2018.2829458.

[14] R. Bojoi, A. Cavagnino, A. Tenconi, and S. Vaschetto, 'Control of Shaft-Line-Embedded Multiphase Starter/Generator for Aero-Engine', *IEEE Trans. Ind. Electron.*, vol. 63, no. 1, pp. 641–652, Jan. 2016, doi: 10.1109/TIE.2015.2472637.

[15] K. Hatua and V. T. Ranganathan, 'Direct torque control schemes for split-phase induction machine', *IEEE Trans. Ind. Appl.*, vol. 41, no. 5, pp. 1243–1254, Sep. 2005, doi: 10.1109/TIA.2005.855043.

[16] G. Pellegrino, R. I. Bojoi, and P. Guglielmi, 'Unified Direct-Flux Vector Control for AC Motor Drives', *IEEE Trans. Ind. Appl.*, vol. 47, no. 5, pp. 2093–2102, Sep. 2011, doi: 10.1109/TIA.2011.2161532.

[17] S. Rubino, 'High Performance Control Techniques for Multiphase eDrives', Doctoral thesis, Politecnico di Torino, 2019.

[18] Y. Hu, Z. Q. Zhu, and M. Odavic, 'Comparison of Two-Individual Current Control and Vector Space Decomposition Control for Dual Three-Phase PMSM', *IEEE Trans. Ind. Appl.*, vol. 53, no. 5, pp. 4483–4492, Sep. 2017, doi: 10.1109/TIA.2017.2703682.

[19] J. Karttunen, S. Kallio, P. Peltoniemi, P. Silventoinen, and O. Pyrhönen, 'Decoupled Vector Control Scheme for Dual Three-Phase Permanent Magnet Synchronous Machines', *IEEE Trans. Ind. Electron.*, vol. 61, no. 5, pp. 2185–2196, May 2014, doi: 10.1109/TIE.2013.2270219.

[20] S. Kallio, M. Andriollo, A. Tortella, and J. Karttunen, 'Decoupled d-q Model of Double-Star Interior-Permanent-Magnet Synchronous Machines', *IEEE Trans. Ind. Electron.*, vol. 60, no. 6, pp. 2486–2494, Jun. 2013, doi: 10.1109/TIE.2012.2216241.

[21] M. Zabaleta, E. Levi, and M. Jones, 'Modelling approaches for triple three-phase permanent magnet machines', in *2016 XXII International Conference on Electrical Machines (ICEM)*, 2016, pp. 466–472, doi: 10.1109/ICELMACH.2016.7732567.

[22] Rubino, S., Bojoi, R., Cittanti, D., and Zarri, L., 'Decoupled Torque Control of Multiple Three-Phase Induction Motor Drives', in *2019 IEEE Energy Conversion Congress and Exposition (ECCE)*, Baltimore (USA), 2019, pp. 1–8.

[23] I. Zoric, M. Jones, and E. Levi, 'Vector space decomposition algorithm for asymmetrical multiphase machines', in *2017 International Symposium on Power Electronics (Ee)*, 2017, pp. 1–6, doi: 10.1109/PEE.2017.8171682.

[24] P. Krause, O. Wasynczuk, S. D. Sudhoff, and S. Pekarek, *Analysis of Electric Machinery and Drive Systems*. John Wiley & Sons, 2013.

[25] I. Zoric, M. Jones, and E. Levi, 'Arbitrary Power Sharing Among Three-Phase Winding Sets of Multiphase Machines', *IEEE Trans. Ind. Electron.*, vol. 65, no. 2, pp. 1128–1139, Feb. 2018, doi: 10.1109/TIE.2017.2733468.

[26] G. Sala, M. Mengoni, G. Rizzoli, L. Zarri, and A. Tani, 'Decoupled d-q Axes Current Sharing Control of Multi Three-Phase Induction Machines', *IEEE Trans. Ind. Electron.*, pp. 1–1, 2019, doi: 10.1109/TIE.2019.2941127.

[27] I. Zoric, M. Jones, and E. Levi, 'Arbitrary d–q current sharing in three-phase winding sets of multi-phase machines', *J. Eng.*, vol. 2019, no. 17, pp. 4173–4177, 2019, doi: 10.1049/joe.2018.8130.

[28] R. Kianinezhad, B. Nahid-Mobarakeh, L. Baghli, F. Betin, and G. Capolino, 'Modeling and Control of Six-Phase Symmetrical Induction Machine Under Fault Condition Due to Open Phases', *IEEE Trans. Ind. Electron.*, vol. 55, no. 5, pp. 1966–1977, May 2008, doi: 10.1109/TIE.2008.918479.

[29] H. Guzman, M. J. Duran, F. Barrero, B. Bogado, and S. Toral, 'Speed Control of Five-Phase Induction Motors With Integrated Open-Phase Fault Operation Using Model-Based Predictive Current Control Techniques', *IEEE Trans. Ind. Electron.*, vol. 61, no. 9, pp. 4474–4484, Sep. 2014, doi: 10.1109/TIE.2013.2289882.

[30] V. Kaura and V. Blasko, 'Operation of a phase locked loop system under distorted utility conditions', *IEEE Trans. Ind. Appl.*, vol. 33, no. 1, pp. 58–63, Jan. 1997, doi: 10.1109/28.567077.

[31] S. Rubino, R. Bojoi, A. Cavagnino, and S. Vaschetto, 'Asymmetrical twelve-phase induction starter/generator for more electric engine in aircraft', in *2016 IEEE Energy Conversion Congress and Exposition (ECCE)*, 2016, pp. 1–8, doi: 10.1109/ECCE.2016.7854889.

[32] G. Rizzoli, G. Serra, P. Maggiore, and A. Tenconi, 'Optimized design of a multiphase induction machine for an open rotor aero-engine shaft-line-embedded starter/generator', in *IECON 2013 - 39th Annual Conference of the IEEE Industrial Electronics Society*, 2013, pp. 5203–5208, doi: 10.1109/IECON.2013.6699980.

[33] F. Mariut, S. Rosu, R. Bojoi, and A. Tenconi, 'Multiphase modular power converter using the PEBB concept and FPGA-based direct high speed voltage measurement', in *2015 17th European Conference on Power Electronics and Applications (EPE'15 ECCE-Europe)*, 2015, pp. 1–10, doi: 10.1109/EPE.2015.7309332.

[34] Sang-Hoon Kim and Seung-Ki Sul, 'Maximum torque control of an induction machine in the field weakening region', *IEEE Trans. Ind. Appl.*, vol. 31, no. 4, pp. 787–794, Jul. 1995, doi: 10.1109/28.395288.